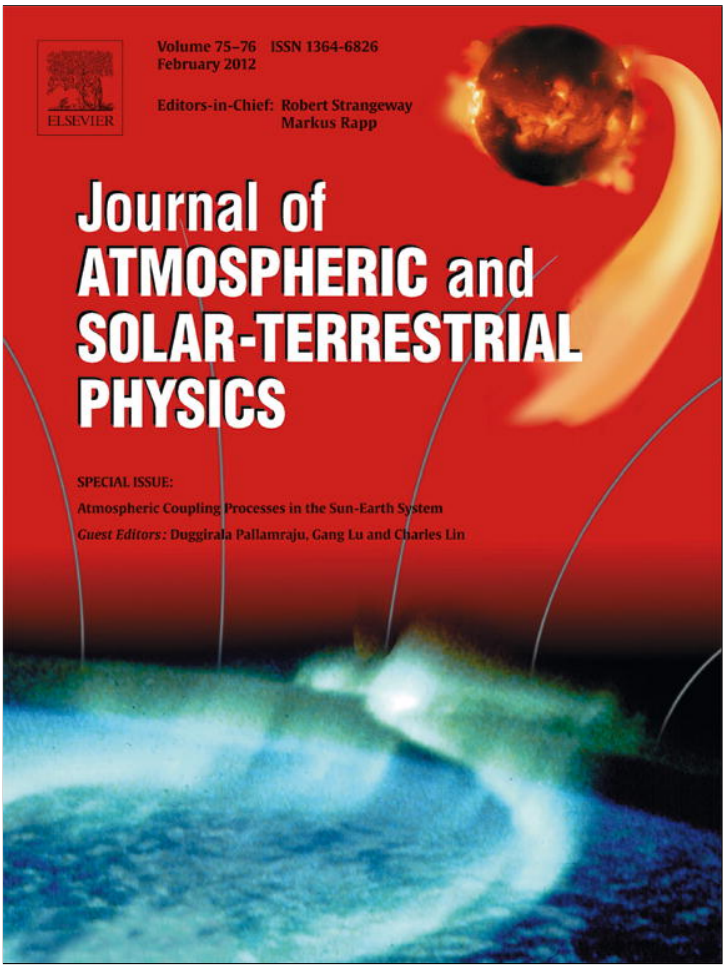

Journal of Atmospheric and Solar-Terrestrial Physics 75–76 (2012) 15–21

Contents lists available at ScienceDirect

Journal of Atmospheric and Solar-Terrestrial Physics

journal homepage: www.elsevier.com/locate/jastp

Study of the influence of magnetic fluctuations and solar plasma density on the solar wind–magnetosphere coupling

Y.P. Singh [a], Badruddin [b,*]

[a] Department of Applied Physics, Mangalayatan University, Aligarh 202145, India
[b] Department of Physics, Aligarh Muslim University, Aligarh 202002, India

ARTICLE INFO

Article history:
Received 5 December 2010
Received in revised form
1 May 2011
Accepted 5 May 2011
Available online 17 June 2011

Keywords:
Solar wind
Geomagnetic storm
Solar wind–magnetosphere coupling

ABSTRACT

We have identified and selected 212 geomagnetic disturbances of varying level of geomagnetic activity, based on the changes in Dst index. The selected events are divided into six different groups according to different geomagnetic activity levels. We study the average behavior of solar plasma flow speed (V), density (N), dynamic pressure (P), magnetic field (B), its north–south component (Bz) and variance (σ_B) and dusk-ward electric field (Ey), and their role in solar wind–magnetosphere coupling. For this purpose we adopted the method of superposed epoch (SPE) analysis. Hourly solar wind plasma and field parameters (V, B, Bz, σ_B, N, P, Ey) together with Dst index are analyzed using SPE analysis with respect to the start of the changes in geomagnetic activity, separately for all six groups of increasing level of activity. In particular, we study the influence of the enhancements in solar plasma density/dynamic pressure and field fluctuations on the solar wind–magnetosphere coupling, during southward field orientation within the responsible interplanetary structures. In addition to studying the average properties with the use of SPE analysis, we have also considered individual events with different level of geomagnetic activity (Dst) and studied its relationship to interplanetary field parameters. We observed that the enhancement in plasma density/pressure and fluctuations in field starting several hours before the storm/activity onset, might play a role in enhancing the solar wind–magnetosphere coupling efficiency.

1. Introduction

Disturbances originating at the sun and traveling through interplanetary space induce explosive processes such as storms in geo-space. Basic research of solar–terrestrial physics in general and solar–magnetosphere coupling, in particular, has long been interesting and attractive. In recent past, this area acquired an applied touch too, (a) due to often harmful effects of solar–terrestrial coupling processes on technological systems, (b) due to increasing indication that solar induced geomagnetic disturbances may be hazardous for human health, and (c) due to possible influence of solar wind/solar activity on weather and climate change (e.g. Daglis et al., 2003).

The most application oriented part of solar–terrestrial research today is space weather forecasting, which is an effort to have reliable means of predicting major geo-space disturbances particularly geomagnetic storms. It requires, among others, a detailed understanding of solar–terrestrial coupling process and ascertaining those factors that are ultimately responsible for geomagnetic storms (e.g. see Kudela et al., 2000; Sabbah, 2000; Kudela and Storini, 2005; Badruddin, 2006; Schwenn, 2006; Kane and Echer, 2007; Echer et al., 2008; Gupta and Badruddin, 2009; Kane, 2010; and references therein).

The principal manifestation of geomagnetic storms, measured by Dst, is the increase of the ring current intensity, which depends upon the reconnection rate (coupling of interplanetary magnetic field (IMF) with the Earth's magnetic field) that allows the solar wind energy transfer into the earth's magnetotail/magnetosphere. It is known that a persistent southward IMF produces increased geomagnetic activity, and the dawn–dusk electric field (VBs) is a critical storm parameter (e.g. Burton et al., 1975; Badruddin, 1998; Mustajab and Badruddin, 2011). However, it is important to know whether enhanced plasma density/dynamic pressure (e.g. Murayama, 1982; Srivastava and Venketakrishnan, 2002; Boudouridis et al., 2005; Xie et al., 2008; Ontiveros and Gonzalez-Esparza, 2010) and/or magnetic irregularities (Garrett et al., 1974; Feldstein, 1992; Kershengolts et al., 2007; Kim et al., 2009; Badruddin et al., 2010) lead to enhanced coupling between the solar wind and terrestrial magnetosphere, significantly increasing the geoeffectiveness of the solar wind. It is also important to know which typical conditions precede all magnetic storms and not only the severe storms (Khabarova and Yermolaev, 2008;

* Corresponding author.
E-mail address: badr_phys@yahoo.co.in (Badruddin).

1364-6826/$ - see front matter © 2011 Elsevier Ltd. All rights reserved.
doi:10.1016/j.jastp.2011.05.005

Badruddin and Singh, 2009). Considering geoeffectiveness of different magnitude as a measure of coupling efficiency/reconnection rate, we study the effects of both the enhanced field fluctuation and the plasma density on the magnetic reconnection/coupling efficiency. We consider solar plasma/field properties, including the field fluctuation (σ_B), plasma density (N) and dynamic pressure (NV^2) before, during and after interplanetary events of geo-space consequences.

2. Method of analysis

We have first made visual inspection of the Dst-time plot of hourly Dst values of each solar rotation for the period 1995–2006. From these plots, we have identified an event when there is a continuous change in Dst towards positive Dst values for some time (≥ 1 day) or toward negative Dst values continuously for some time (≤ 1 day). We use the more general term 'geomagnetic events' as those with Dst ≥ 0 nT are geomagnetically quiet events, not geomagnetic storms.

After selecting geomagnetic disturbances of varying geomagnetic activity, we have grouped them according to the level of geomagnetic activity as: group I (quiet; Dst ≥ 0 nT), group II (very low; -30 nT $\leq$ Dst < 0 nT), group III (low; -50 nT $\leq$ Dst < -30 nT), group IV (moderate; -100 nT $\leq$ Dst < -50 nT), group V (high; -150 nT $\leq$ Dst < -100 nT) and groupVI (very high; Dst < -150 nT).

Based on the above criteria, we have analyzed the solar wind plasma and field behavior before, during and after these periods of varying geomagnetic activity. The solar wind parameters selected for this study are; solar plasma flow speed (V), density (N), dynamic pressure (P), magnetic field (B), its north–south component (Bz) and its variance (σ_B), and duskward electric field (Ey). The index Dst is the geomagnetic activity parameter selected for deciding the level of geomagnetic activity.

To study the average behavior of these parameters and their role in solar wind–magnetosphere coupling, we have first adopted the method of superposed epoch (SPE) analysis. Hourly solar wind plasma and field parameters (V, B, Bz, σ_B, N, P, Ey) together with Dst index are analyzed using SPE analysis with respect to the start of activity separately for all six groups with increasing level of activity.

The superposed epoch analysis is valuable in showing the average behavior of the system, e.g. average Dst response to increase in velocity of the solar wind. Given proper physical insight in the choice of parameters and in the selection of zero-epoch time, the superposed epoch method can be very valuable addition to cross-correlation studies (Badruddin, 1998; Singh and Badruddin, 2006). Therefore cross-correlation analysis between Dst and solar wind parameters –Bz/Ey has also been performed. A few typical individual events have also been analyzed.

3. Results

In Figs. 1–3, we have plotted the results of the superposed epoch analysis showing average behavior of different solar wind parameters (V, B, Bz, σ_B, N, P and Ey) alongwith a geomagnetic index (Dst) during periods of different geomagnetic activity.

Fig. 1 (left panel) is a superposed epoch plot showing variations in different parameters (V, B, Bz, σ_B, N, P, Ey and Dst) 48 h before and 72 h after the start of all the 35 group-I events with Dst ≥ 0 nT. This start time is shown by a vertical line at zero hour. The gray hatched area in the panel highlights the duration around (before/after) zero time, from the start of the increase/decrease to the maximum or minimum (as the case may be) in each parameter plotted in the figure. The average behavior of solar wind parameters during quiet geomagnetic activity (Dst ≥ 0 nT) can be summarized as follows: solar wind velocity is very low, Bz is northward (positive) and Ey is negative. Although increasing, the enhancement in some of the parameters (B, σ_B, N and P) is very slow and small in magnitude during geomagnetically quiet period**s** (Dst ≥ 0 nT). Moreover, the enhancement of these parameters starts somewhat later, 3–6 h after the event onset.

In the right panel of Fig. 1, we have plotted the results of SPE analysis showing the variations in different solar/plasma field variations before and after the onset of geomagnetic disturbances of group-II (-30 nT $\leq$ Dst < 0 nT). The onset corresponds to zero hour on the time scale. The gray hatched area highlight the duration from the start of the decrease/increase to the maximum/minimum (as the case may be) in each parameter, around the onset time. From these averaged plots obtained with reference to very low geomagnetic activity events, we see that there are small changes in all the solar wind parameters. The Bz changes from positive to negative and Ey from negative to positive value, small increase in all other parameters (V, B, σ_B, N, and P) with fluctuations in the magnetic field are also observed. Moreover, the enhancement in all these parameters starts before the onset of the geomagnetic disturbance, peak values reached close to onset

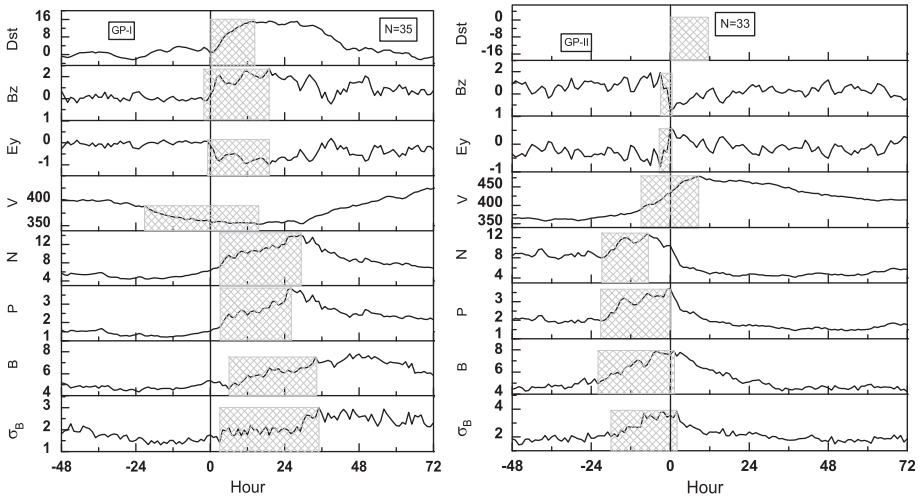

Fig. 1. Average behavior of interplanetary plasma field parameters namely magnetic field (nT), its variance (nT), dynamic pressure (nPa), density (n/cc), plasma flow speed (km/s), dusk-ward electric field (mV/m), north–south component of magnetic field (nT) during geomagnetically quite activity (Dst ≥ 0 nT) periods (left panel), and during geomagnetically very low activity (-30 nT $\leq$ Dst < 0 nT) periods (right panel).

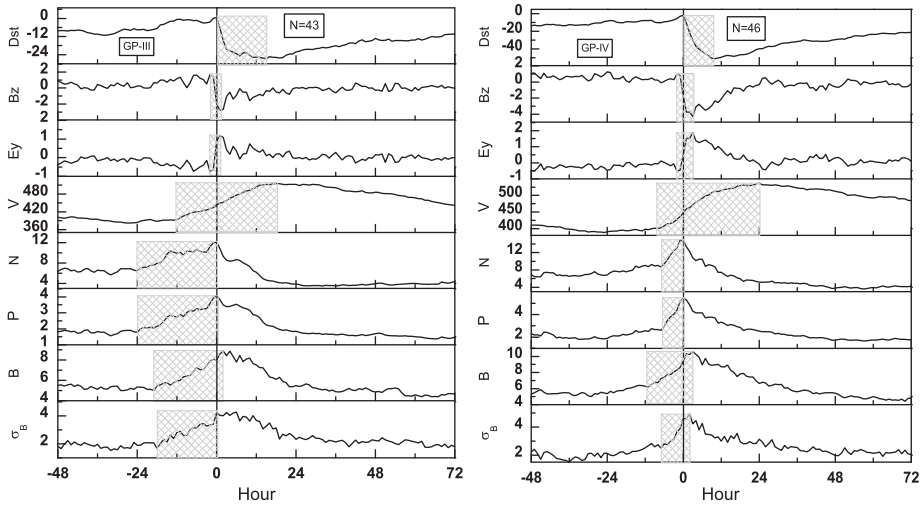

Fig. 2. Same as Fig. 1 but during geomagnetically low activity (-50 nT $\leq$ Dst <-30 nT) periods (left panel), and during moderately geo-active (-100 nT $\leq$ Dst <-50 nT) periods (right panel).

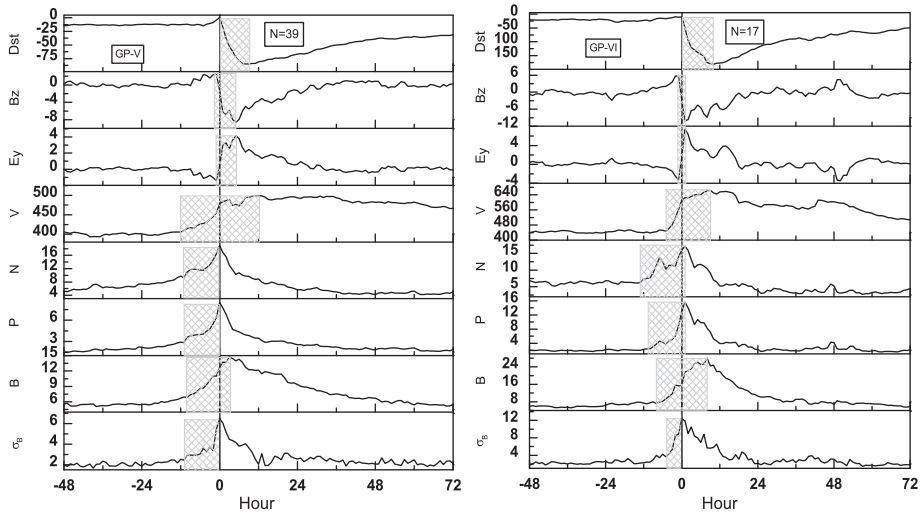

Fig. 3. Average behavior of interplanetary plasma field parameters during highly geo-active (-150 nT $\leq$ Dst <-100 nT) periods (left panel) and during geomagnetically very highly active (Dst <-150 nT) periods (right panel).

(B, Bz, σ_B, P and Ey), before (P) or after (V) the event onset i.e. zero hour.

The SPE plots with respect to group-III (-50 nT $\leq$ Dst <-30 nT) and group-IV (-100 nT $\leq$ Dst <-50 nT) geomagnetic disturbances are shown, respectively, in the left and the right panels of Fig. 2. The change in sign in Bz, Ey near the onset time (zero hour) and enhancements in parameters N, P, B and σ_B are starting several hours before and reaching their peaks around the onset time with increasing velocity, density, pressure, field strength; moreover the field is fluctuating too.

In Fig. 3, we have plotted the SPE result with respect to group-V (-150 nT $\leq$ Dst <-100 nT) and group-VI (Dst <-150 nT) geomagnetic disturbances showing variations in solar plasma and field parameters 48 h before and 72 h after the onset of disturbances. In addition to change in all the parameters with greater magnitude, starting several hours before the onset of geomagnetic disturbances, particularly in N, P and B, the field is fluctuating and σ_B is maximum at/around the onset.

Table 1 summarizes the average values of geomagnetic and plasma/field parameters at the start (represented by subscript 'o' with each parameter) of the increase/decrease and at maximum/minimum (represented by subscript 'm' with each parameter). In addition to change in the direction of Bz (positive to negative) and Ey (negative to positive), the increase in plasma velocity, density and pressure, enhancement in field magnitude and fluctuation in it are also evident from this table.

Table 2 shows the lag/lead time (in hours), with respect to onset of geomagnetic activity (zero hour) of each parameter. The time Δt_o of each parameter represent the time of start of change, and Δt_m is the time of maximum/minimum before ($-$) or after ($+$) the activity onset time. We see that, on the averages, the enhancement in N, P and σ_B starts a few hours ($\sim$3 h) after the event onset in the case of group-I (quiet activity) events. Moreover, these parameters attain their maximum value about 25–35 h after the onset time. However, in the case of geomagnetically disturbed groups (group II–VI) of varying activity, the enhancement in three parameters (N, P and σ_B) starts before the onset and reaches the maximum values around the onset time. The density and pressure enhancements in different active groups (II–VI) start 6–24 h before the onset time and reach their respective maximum

Table 1
Average values (SEP results) of different parameters at the start (represented by subscript 'o' with each parameter) and at the maximum/minimum (represented by subscript 'm' with each parameter).

Activity group	Dst (nT)		Bz (nT)		B (nT)		σ_B (nT)		N (n/cc)		V (km/s)		Ey (mV/m)		P (nPa)	
	Dst_o	Dst_m	Bz_o	Bz_m	B_o	B_m	σ_{Bo}	σ_{Bm}	N_o	N_m	V_o	V_m	Ey_o	Ey_m	P_o	P_m
I	1	15	−0.2	2.7	4.6	7.5	1.4	3.0	8.0	14.1	389	353	0.1	−1.0	2.0	3.9
II	1	−17	1.1	−1.9	4.9	7.9	2.0	3.8	8.0	12.8	358	478	−0.8	0.6	2.0	3.7
III	0	−27	1.7	−2.8	5.0	8.9	1.7	4.0	6.4	12.0	391	516	−0.8	1.2	1.8	4.0
IV	0	−51	0.8	−3.7	5.5	10.6	2.7	4.9	8.7	14.9	401	537	−0.5	1.9	2.6	5.5
V	1	−85	3.0	−7.6	5.9	14.7	2.9	6.5	7.2	19.0	405	499	−1.4	3.8	2.8	8.5
VI	−11	−180	5.9	−7.7	7.2	28.0	3.6	12.3	6.1	17.2	447	664	−3.3	7.5	3.7	15.8

Table 2
Lead/lag time (in hours) of minimum and maximum values of different parameters with respect to onset of Dst (zero hour). Time in (−) means before and (+) means after the Dst onset time (zero hour).

Activity group	Dst (nT)		Bz (nT)		B (nT)		σ_B (nT)		N (n/cc)		V (km/s)		Ey (mV/m)		P (nPa)	
	Δt_o	Δt_m	Δt_o	Δt_m	Δt_o	Δt_m	Δt_o	Δt_m	Δt_o	Δt_m	Δt_o	Δt_m	Δt_o	Δt_m	Δt_o	Δt_m
I	0	+15	−2	+19	+6	+34	+3	+35	+3	+29	−21	+16	−1	+19	+3	+26
II	0	+11	−3	0	−22	+1	−16	−2	−21	−7	−9	+9	−3	0	−21	0
III	0	+15	−2	+1	−19	+2	−18	0	−24	0	−12	+18	−2	+1	−24	0
IV	0	+10	−2	+3	−11	+3	−5	+2	−7	−1	−8	+24	−2	+3	−7	0
V	0	+9	−2	+5	−10	+3	−10	0	−22	0	−12	+12	−1	+6	−11	0
VI	0	+10	−2	+2	−7	+8	−5	0	−14	+1	−5	+10	−1	+1	−11	+1

Table 3
Change in parameters (in respective units) and corresponding duration ΔT (hours) during different activity levels.

Activity group	Dst (nT)		Bz (nT)		B (nT)		σ_B (nT)		N (n/cc)		V (km/s)		Ey (mV/m)		P (nPa)	
	ΔDst	ΔT	ΔBz	ΔT	ΔB	ΔT	$\Delta\sigma_B$	ΔT	ΔN	ΔT	ΔV	ΔT	ΔEy	ΔT	ΔP	ΔT
I	14	15	2.9	21	2.9	28	1.6	32	6.1	39	−36	−35	−1.1	20	1.9	28
II	−16	11	−3.0	3	3.0	23	1.8	14	4.8	28	120	18	1.4	3	1.7	21
III	−26	15	−4.5	3	3.9	21	2.3	18	5.7	24	125	30	1.9	3	2.3	24
IV	−51	10	−4.5	5	5.1	14	2.2	7	6.2	6	136	32	2.4	5	2.9	7
V	−84	9	−10.6	7	8.8	13	3.6	10	11.7	22	94	24	5.2	7	5.7	11
VI	−191	10	−13.6	4	20.9	15	8.7	5	11.1	15	217	15	10.8	2	11.9	12

values around the onset (within ±1 h in almost all cases). The increase in σ_B also starts earlier (5–18 h) and maximum value is around the onset (±2 h).

Table 3 depicts the average amplitude of various parameters and the time taken to reach the maximum/minimum from the start of change in each parameter. These averaged values for each activity group (I–VI) show, in general, increasing values not only in V, Bz and Ey but also in N, P, B and σ_B, with increasing level of geomagnetic activity.

Thus during geomagnetically active periods of successively increasing geomagnetic activity (−30 nT ≤ Dst < 0 nT; −50 nT ≤ Dst < −30 nT; −100 nT ≤ Dst < −50 nT; −150 nT ≤ Dst < −100 nT and Dst < −150 nT), Bz is turning southward and Ey suddenly increases(see Figs. 1–3). The average values of geomagnetic as well as interplanetary plasma and field parameters vary. An observation of special mention from these figures is that N, P and σ_B start increasing 6–24 h earlier than the onset of activity, reach their maximum values at/near the onset of the activity, and then decrease. In other words, significant solar wind–magnetosphere coupling takes place at the peak of N, P and σ_B, together with intensification of southward field (−Bz) and duskward electric field (Ey). These behaviors are observed in all five geo-magnetically active groups (group II–VI) with varying degree lead/lag time.

Although averaged and grouped plots shown in Figs. 1–3 indicate that enhancement in plasma density/pressure and fluctuations in field, before the storm/activity onset, might play a role in solar wind–magnetosphere coupling, the average enhancements in almost all the parameters (V, B, Bz, σ_B, Ey, N, P) appear related to the level of geomagnetic activity as represented by the change in Dst in different activity level groups. However, scatter plots of 165 events between Dst and Bz (Fig. 4 (left panel)) and between Dst and Ey (right panel of Fig. 4) show a number of events with almost the same −Bz or Ey but with quite different storm intensity (−Dst). Also, there are storms with the same amplitude produced by events of quite different −Bz (Ey) intensity (see gray shaded portions in Fig. 4). These events provide sufficient ground to look for the possible role of some additional parameters in the intensification of a storm (or enhancing the coupling efficiency).

We have selected three sets of typically observed events (with two events in each set), having comparable Bz/Ey/ V/B. These events are shown in Figs. 5–7(A) and (B).

Fig. 5(A) and (B) are the plots for two individual geomagnetic events with nearly same (−Bz) and V, but with different geomagnetic response; one producing a storm of magnitude twice that of other. We can see a marked difference in density, pressure and field fluctuations; these parameters are much larger in case of geomagnetic disturbance of larger magnitude and also the enhancements in these parameters start much earlier (see Fig. 5(A) and (B)). The amplitudes of different parameters are tabulated (see, Set-I event values in Table 4). We see from Table 4, that for the two set-I events, Bz is nearly same (−15.1 and

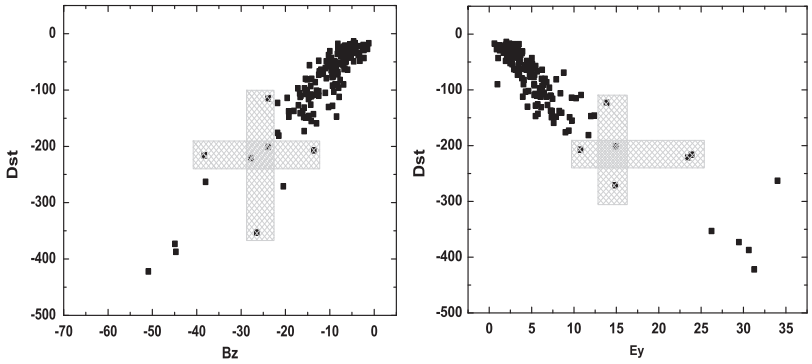

Fig. 4. Scatter plot between Dst (nT) and Bz (nT) (left panel) and Dst (nT) versus Ey (mV/m) (right panel).

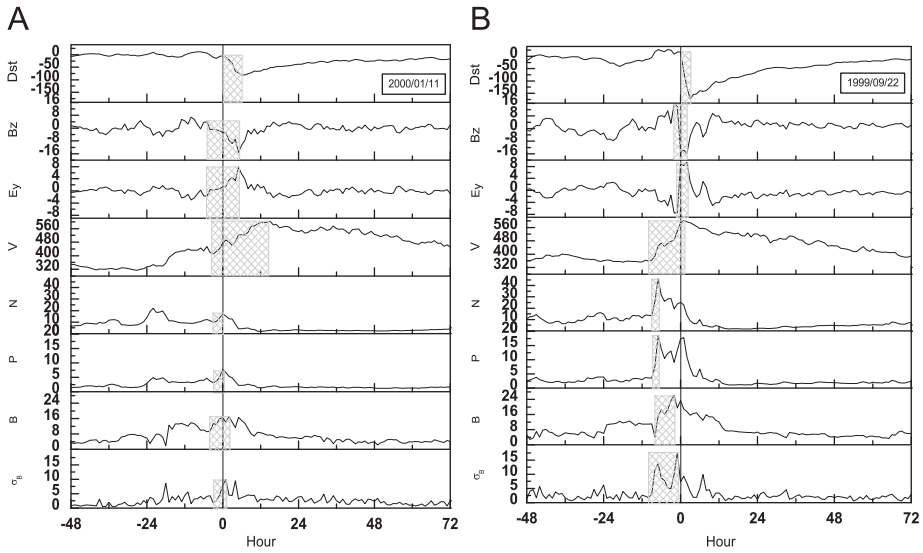

Fig. 5. Two events with nearly equal −Bz (nT) and V (km/s) with different geomagnetic response.

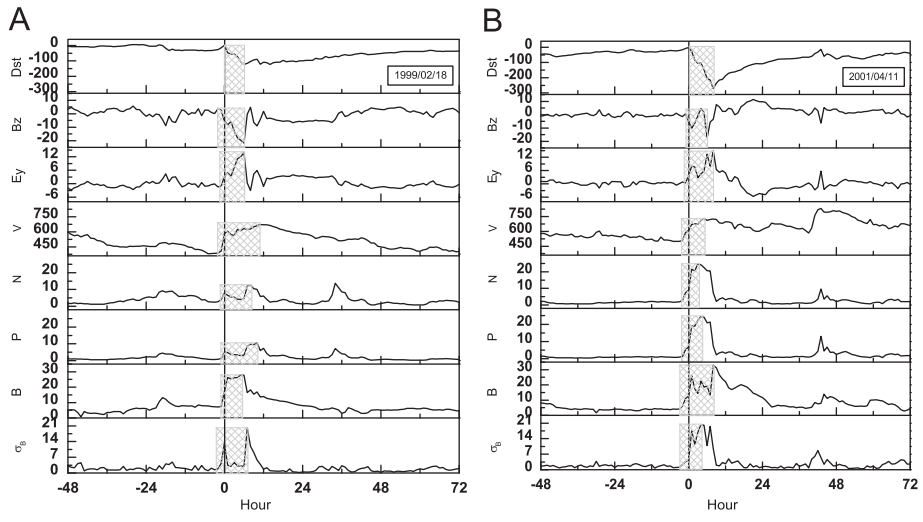

Fig. 6. Two events with nearly the same −Ey (mV/m) but different geomagnetic response.

−15.8 nT), *V* is also equal (602 and 602 km/s), and the amplitude of Ey is also not much different for these two events (7.9 and 9.4 mV/m). But the amplitudes of *N* and σ_B, in particular, are larger by a factor of 3 ($N\sim$17.7 and 46.0 n/cm^3; $\sigma_B\sim$4.6 and 17.7 nT) in case of the stronger storm (Dst∼–173 nT) as compared to the weaker storm (Dst∼ –81 nT).

Fig. 6(A) and (B) shows a set of two geomagnetic events with nearly same Ey (13.8 and 14.9 mV/m; see Set-II events in Table 4). In spite of a larger value of Bz (−21.8 nT) for the event shown in Fig. 6(A) as compared to that shown in Fig. 6(B) (Bz∼ −17.7 nT) the geomagnetic disturbance is about twice (Dst∼ −271 nT) in case of the latter event as compared to the former event (Dst∼ −123 nT).

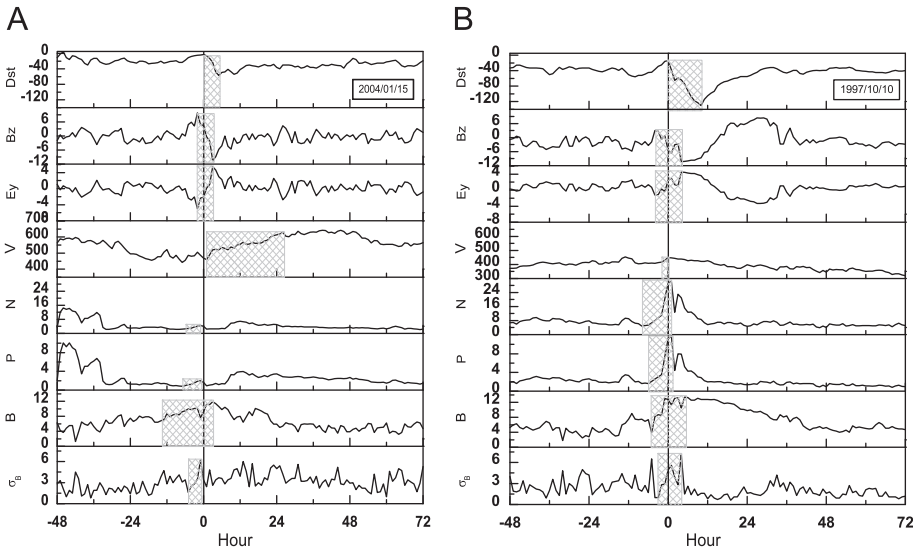

Fig. 7. Two events with nearly equal −Bz (nT) with different geomagnetic activity.

Table 4
Comparison of solar wind and geomagnetic parameters for three set of individual events.

Parameters	Set-I (events)		Set-II (events)		Set-III (events)	
	2000/01/11	1999/09/22	1999/02/18	2001/04/11	2004/01/15	1997/10/10
Dst (nT)	−81	−173	−123	−271	−57	−130
Bz (nT)	−15.1	−15.8	−21.8	−17.7	−10.5	−10.3
Ey (mV/m)	7.9	9.4	13.8	14.9	5.4	4.4
V (km/s)	602	602	673	725	535	449
B (nT)	17.1	26.2	28.1	33.1	11.9	13.2
N (n/cc)	17.1	46.0	12.7	24.7	4.5	30.2
P (nPa)	7.7	18.6	10.7	24.5	2.0	11.8
σ_B (nT)	4.6	17.7	11.9	20.3	6.2	5.6

However, the enhancements in σ_B (20.3 against 11.9 nT) and *N* (24.7 against 12.7 n/cm^3) are almost double in the case of the more geo-active event (with Dst∼ −271 against −123 nT).

We have plotted another set of two events in Fig. 7(A) and (B) with equal Bz (∼−10.5 and −10.3 nT). In spite of slightly higher Ey (5.4 against 4.4 mV/m) and velocity (535 against 449 km/s) for the first event (Fig. 7(A)), the event shown in Fig. 7(B) is geomagnetically much active (Dst∼−130 nT) than that shown in Fig. 7(A) (see Table 4, Set-III events). However, in the case of the more geo-active event, there is an enhancement of about a factor of 6 in *N* (30.2 against 4.5 n/cm^3), and consequently *P* (11.8 against 2.0 nPa); the enhancement in *N* starting several hours before the onset of geomagnetic storm of Dst∼ −130 nT.

Figs. 5–7 (and Table 4) further show more explicitly that an enhancement in plasma density/dynamic pressure and field fluctuations make an additional impact; apparently enhance the coupling efficiency between the interplanetary and magnetospheric fields, increasing the reconnection rate and energy transfer to the magnetosphere from the solar wind.

4. Conclusions

We provide evidence that the enhanced plasma density/dynamic pressure and field fluctuations aid the reconnection between the solar wind and magnetospheric field, enhancing the coupling efficiency and energy transfer from the solar wind to the magnetosphere. The enhancements in *N*, *P* and σ_B, start 6–24 h before the onset of the geomagnetic activity, on the average, and these may be useful parameters for space weather forecast.

Acknowledgments

Use of NASA/OMNIWeb-based solar wind plasma and field data is gratefully acknowledged. We thank the two anonymous reviewers for their helpful comments and suggestions.

References

Badruddin, 1998. Interplanetary shocks, magnetic clouds, stream interfaces and resulting geomagnetic disturbances. Planetary and Space Science 46, 1015.
Badruddin, 2006. Transient perturbations and their effects in the heliosphere, the geo-magnetosphere, and the earth's atmosphere: Space weather perspective. Journal of Astrophysics and Astronomy 27, 209.
Badruddin, Singh, Y.P., 2009. Geoeffectiveness of magnetic cloud, shock/sheath, interaction region, high-speed stream and their combined occurrence. Planetary and Space Science 57, 318.
Badruddin, Gupta, V., Singh, Y.P., 2010. Coupling of the solar wind and the magnetosphere. In: Hasan, S.S., Rutten, R.J. (Eds.), Magnetic Coupling Between the Interior and Atmosphere of the Sun. Springer-Verlag, Berlin Heidelberg, pp. 533.
Boudouridis, A., Zesta, E., Lyons, L.R., Anderson, P.C., Lummerzheim, D., 2005. Enhanced solar wind geoeffectiveness after a sudden increase in dynamic pressure during southward IMF orientation. Journal of Geophysical Research 110, A05214. doi:10.1029/2004JA010704.
Burton, R.K., McPherron, R.L., Russel, C.T., 1975. An Empirical relationship between interplanetary conditions and Dst. Journal of Geophysical Research 80, 4204.
Daglis, I.A., Kozyra, J.U., Kamide, Y., Vassiliadis, D., Sharma, A.S., Liemohn, M.W., Gonzalez, W.D., Tsurutani, B.T., Lu, G., 2003. Intense space storms: critical

issues and open disputes. Journal of Geophysical Research 108, 1208. doi:10.1029/2002JA009722.
Echer, E., Gonzalez, W.D., Tsurutani, B.T., Gonzalez, A.L.C., 2008. Interplanetary conditions causing intense geomagnetic storms ($Dst \leq -100$ nT) during solar cycle 23 (1996–2006). Journal of Geophysical Research 113, A05221. doi:10.1029/2007JA012744.
Garrett, H.B., Dessler, A.J., Hill, T.W., 1974. Influence of solar wind variability on geomagnetic activity. Journal of Geophysical Research 79, 4603.
Gupta, V., Badruddin, 2009. Interplanetary structures and solar wind behavior during major geomagnetic perturbations. Journal of Atmospheric and Solar Terrestrial Physics 71, 885.
Feldstein, Y.I., 1992. Modeling of the magnetic field of magnetospheric ring current as a function of interplanetary parameters. Space Science Reviews 59, 83.
Kane, R.P., Echer, E., 2007. Phase shift (time) between storm-time maximum negative excursions of geomagnetic disturbance index Dst and interplanetary Bz. Journal of Atmospheric and Solar Terrestrial Physics 69, 1009.
Kane, R.P., 2010. Relationship between the geomagnetic Dst(min) and the Interplanetary Bz(min) during cycle 23. Planetary Space Science 58, 392.
Kershengolts, S.Z., Barkova, E.S., Plotnikov, I.Ya., 2007. Dependence of geomagnetic disturbances on extreme values of the solar wind Ey component. Geomagnetism and Aeronomy 47, 167.
Khabarova, O.V., Yermolaev, Y.I., 2008. Solar wind parameters behavior before and after magnetic storms. Journal of Atmospheric and Solar-Terrestrial Physics 70, 384.
Kim, H.–J., Lyons, L.R., Zou, S., Boudouridis, A., Lee, D.–Y., Heinselman, C., McCready, M., 2009. Evidence that solar wind fluctuations substantially affect the strength of dayside ionospheric convection. Journal of Geophysical Research 114, A11305.
Kudela, K., Storini, M., Hofer, M.Y., Belov, A.V., 2000. Cosmic rays in relation to space weather. Space Science Reviews 93, 153.
Kudela, K., Storini, M., 2005. Cosmic ray variability and geomagnetic activity: a statistical study. Journal of Atmospheric and Solar-Terrestrial Physics 67, 907.
Mustajab, F., Badruddin, 2011. Geoeffectiveness of the interplanetary manifestations of coronal mass ejections and solar-wind stream–stream interactions. Astrophysics and Space Science 331, 91.
Murayama, T., 1982. Coupling function between solar wind parameters and geomagnetic indices. Review Geophysics and Space Physics 20, 623.
Ontiveros, V., Gonzalez-Esparza, J.A., 2010. Geomagnetic storms caused by shocks and ICMEs. Journal of Geophysical Research 115, A10244.
Sabbah, I., 2000. The role of interplanetary magnetic field and solar wind in modulating both galactic cosmic rays and geomagnetic activity. Journal of Geophysical Research 27, 1823.
Schwenn, R., 2006. Space weather: the solar perspective. Living Reviews in Solar Physics 3, 2006 irsp-2006-2.
Singh, Y.P., Badruddin, 2006. Statistical considerations in superposed epoch analysis and its applications in space research. Journal of Atmospheric and Solar-Terrestrial Physics 68, 803.
Srivastava, N., Venketakrishnan, P., 2002. Relationship between CME speed and geomagnetic storm intensity. Geophysical Research Letters 29, 1287.
Xie, H., Gopalswamy St., N., Cyr, O.C., Yashiro, S., 2008. Effects of solar wind dynamic pressure and preconditioning on large geomagnetic storms. Geophysical Research Letters 35, L06508.